Ocean Systems Engineering, *Vol. 12, No. 1 (2022) 39-61*
https://doi.org/10.12989/ose.2022.12.1.039

Performance of integrated vertical raft-type WEC and floating breakwater

Zhi Yung Tay* and Luke Lee

Engineering Cluster, Singapore Institute of Technology, 10 Dover Drive, Singapore 138683

(Received October 1, 2021, Revised January 26, 2022, Accepted February 16, 2022)

Abstract. Renewable energy such as wave energy has gained popularity as a means of reducing greenhouse gases. However, the high cost and lack of available sea space in some countries have hindered the deployment of wave energy converters (WEC) as alternative means of sustainable energy production. By combining WECs with infrastructures such as floating breakwaters or piers, the idea of electricity generated from WECs will be more appealing. This paper considers the integration of vertical raft-type WEC (commonly known as the vertical flap WEC) with floating breakwater as means to generate electricity and attenuate wave force in the tropical sea. An array of 25 WECs attached to a floating breakwater is considered where their performance and effect on the wave climate are presented. The effects of varying dimensions of the WEC and mooring system of the floating breakwater have on the energy generation are investigated. The integrated WECs and floating breakwater is subjected to both the regular and irregular waves in the tropical sea to assess the performance of the system. The result shows that the integrated vertical flap-floating breakwater system can generate a substantial amount of wave energy and at the same time attenuate the wave force effectively for the tropical sea when optimal dimensions of the WECs are used.

Keywords: flap WEC; integrate WEC and floating breakwater; raft-type WEC; regular wave; uni-directional irregular waves

1. Introduction

With rising concerns about global warming caused by greenhouse gases (Kweku *et al.* 2017, Shine *et al.* 2005), renewable energy has gained popularity as a means of reducing greenhouse gas emissions (Owusu and Asumadu-Sarkodie 2016, Quaschning 2019). There are many sources of renewable energy such as wind energy (Herbert *et al.* 2007), solar energy (Herbert *et al.* 2007), biomass (Chum and Overend 2001) and ocean thermal energy (Wang *et al.*2011) being considered in the past decades as alternatives to hydrocarbon. Wave energy being the relatively new renewable has a high potential due to its greater energy density as compared to wind and solar energy (Falnes 2007). However, the application of wave energy converters (WEC) in island nations such as Singapore and Indonesia is challenging due to their busy sea space as important international maritime routes, thereby also result in difficulty in the installation and deployment of the WECs (Tay 2020). In addition, the capital cost of WECs is high as compared to the conventional energy

*Corresponding author, Associate Professor, E-mail: zhiyung.tay@singaporetech.edu.sg
[a] B.Eng., Student, E-mail: 1801145@sit.singaporetech.edu.sg

http://www.techno-press.org/?journal=ose&subpage=7 ISSN: 2093-6702 (Print), 2093-677X (Online)

production (e.g., coal and gas) or other renewables (e.g., solar and wind), therefore making deployment of WECs in the precious sea space for the sole purpose of generating electricity impractical (Astariz and Iglesias 2015). Nonetheless, the total yearly wave energy potential for tropical countries such as Indonesia is projected to be at 540 GW (Quirapas *et al.* 2015), thus the wave energy presents a viable option as an alternative to fossil fuel in meeting the country's energy demand.

On the other hand, the impacts of coastal erosion caused by the rise in seawater levels have pushed the need to develop technologies in mitigating such damage. Conventionally, the strategies to manage coastal erosion are by retreating or relocating to regions that are higher such as the highland, or by preserving the shoreline with hard structures such as dikes and shore protection materials (Headland *et al.* 2007, Pilarczyk and Press 1990, Schoonees *et al.* 2019). Although shore protection materials such as geotextile (Hornsey *et al.* 2011, Shin and Oh 2007) provide a considerable advantage due to their relatively easy deployment, they may be more expensive compared to the use of hard construction structures such as breakwater (Van Rijn 2011). To optimize the sea space, WECs such as oscillating water column WEC, point absorber WEC and raft-type (attenuator) WEC are proposed to be integrated into breakwater as means to generate energy while attenuating the wave force (He *et al.* 2013, Howe *et al.* 2020a, Nin *et al.* 2016, Zhao *et al.* 2019). While bottom-mounted breakwater is commonly used, floating breakwater (Drimer *et al.* 1992, Williams *et al.* 1991) has been proposed and built due to its cheaper construction costs, environmental friendliness and greater adaptability to the rise of seawater level (McCartney 1985). The concept of integrating WECs with infrastructures (Martinelli *et al.* 2016) (Cabral *et al.* 2020, Howe *et al.* 2020b) such as a pier, breakwater or floating platform enables optimal ocean space utilization and would make the use of WEC as a source of renewable energy more appealing and cost-effective.

Various ideas have therefore been developed to ensure that the WEC will remain competitive in generating energy, e.g., utilizing the effect of resonance for power enhancement of WEC arrays (Tay 2021, 2022a, b), enhancing power energy efficiency using a trilinear-damper system (Chen *et al.* 2021), integration of oscillating buoy type wave energy converter with vertical pile-restrained floating breakwater (FB) proposed by Ning *et al.* (2016) that provides a promising concept to utilize the wave energy cost-effectively. There are also many attempts to combine WECs and floating breakwaters by attaching the WECs at the weather side of the breakwater (Favaretto *et al.* 2017, Martinelli *et al.* 2016). Attenuator type WECs (also known as the raft-type WEC or the flap WEC) that generates energy via pitching motions have also been proposed, e.g., the raft-type WEC attached to a very large floating structure (VLFS) (Tay 2017, 2019). The raft-type WEC shows that the power generation is significantly affected by the length of the plate-like WEC and power take-off (PTO) damping. An optimal design with its resonance frequencies tuned to the wave periods of the irregular waves is important to ensure that the WEC is viable in generating wave energy. The effectiveness of the raft-type WEC could be further enhanced by considering a modular system as proposed by Wilkinson *et al*. (2017). The modular system enables a greater energy extraction from waves arriving at multi-directional seas. In view of this, a novel modular system that comprises multiple raft-type WECs was proposed by Tay (2020) to be integrated with a floating breakwater for the tropical sea. An appropriately sized WECs attached to the floating breakwater was shown to function effectively both as a wave energy converter and floating breakwater in the tropical climate. Different concepts of utilizing pitching motion have also been proposed by Nguyen and Wang (2020) that devised a single vertical oscillating wave surge converter (OWSC) to be integrated with a VLFS. The study investigated the effect of wavelength and PTO damping has on the power production where they

found that the proposed concept as wave energy device and breakwater is promising for deployment in sea state of intermediate and long waves.

In view of the effectiveness of the integrated WECs with nearshore infrastructure, this paper proposes an integrated vertical flap (VF) with floating breakwater (FB) suitable for deployment in the tropical climate. This paper aims to optimize the dimensions of the flap for maximum power generation and wave attenuation effectiveness. A numerical model is built using the hydrodynamic software ANSYS AQWA (2012). The numerical model is first used to study the effects of the mooring system of the floating breakwater, varying length and width of the flap have on the power generation under regular waves. With the optimal dimensions obtained, an array of 25 VF attached to a 50 m length FB is then considered where its power generation and wave attenuation effectiveness under regular waves are studied. Lastly, the significant average power generation is calculated for uni-directional irregular waves, by taking the sea state of the Singapore sea as a case study.

2. Integrated vertical flap-floating breakwater (iVF-FB)

The integrated vertical flap-floating breakwater (known hereafter as iVF-FB) comprises an array of equally spaced VFs hinged on supporting frames attached to the box-like FB as shown in Figs. 1 and 2. The VF operates following the same mechanism as the OWSC, except that it is an inverted OWSC. Figs. 1 and 2 show that the iVF-FB floating on a $X-Y$ plane surface with $Z=0$ representing the free surface. The global origin of the cartesian coordinates is located at the center of the flotation of the FB. As waves hit on the vertical flap (VF), the vertical flaps rotate at an angle Θ_y about the hinge (rotation about the local y-axis, see Fig. 2) where power take-off (PTO) systems are used to convert the mechanical motion into electricity. Twenty-Five VFs are considered in the 50-meter long iVF-FB, where each VF has a length L_{WEC}, width W_{WEC} and thickness t_{WEC}. The dimension and properties of the VF summarized in Table 1 are the optimal value obtained from the parametric studies conducted in Section 5.1. The FB has a length of $L_{FB}=50$ m, width $W_{FB}=3$m and depth $d_{FB}=2$m. The floating breakwater is allowed to move vertically (heave motion) but with its horizontal motions (sway and surge) constrained.

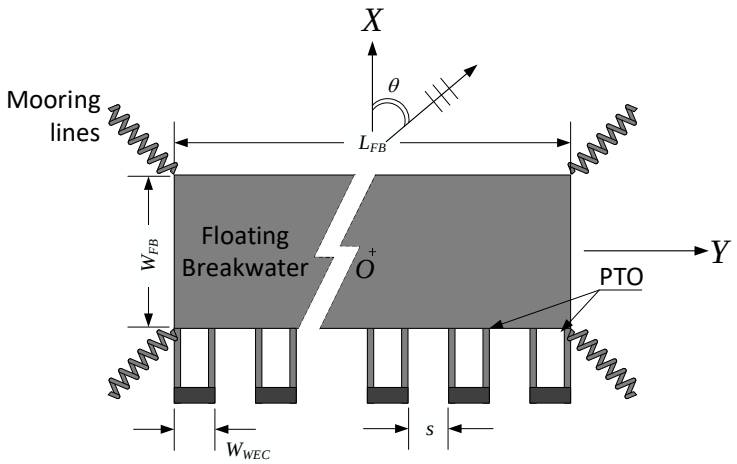

Fig. 1 Plan view of iVF-FB

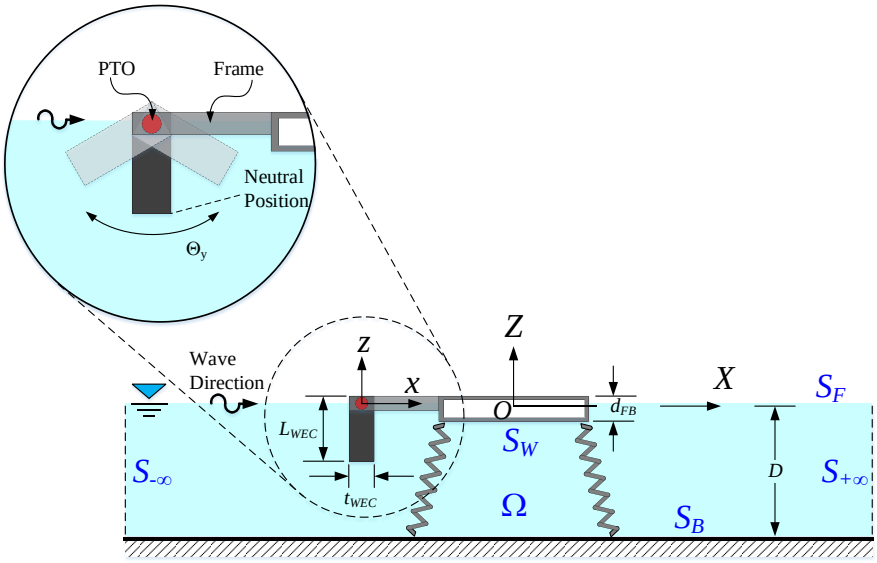

Fig. 2 Elevated view of iVF-FB showing main dimensions and mechanism of WEC in generating wave energy

Table 1 Dimensions and properties of iVF-FB

Components	Symbols	Value
Floating Breakwater	Length, L_{FB} (m)	50.00
	Width, W_{FB} (m)	3.00
	Draft, d_{FB} (m)	2.00
Wave Energy Converter	Number, N	25
	Length, L_{WEC} (m)	2.00
	Thickness, t_{WEC} (m)	0.40
	Width, W_{WEC} (m)	1.25
	PTO damping B_{PTO} (N.m.s/rad)	5913
Regular wave	Wave frequency, ω (rad/s)	1.0 to 6.0
	Wave direction, θ (°)	180, -135
	Water depth, D (m)	10
Irregular wave	Peak Period, T_p (s)	3,4,5,6
	Significant wave height, H_s (m)	2.0

The iVF-FB is subjected to both regular and irregular waves. For both the regular wave and irregular waves analyses, a constant water depth of $D = 10$ m is considered. A parametric study is first performed where a single VF attached to a short FB under a regular wave is considered. The objective of the parametric study is to determine the suitable mooring system of the FB as well as the optimal length and width of VF. The regular wave with a wave amplitude A and wave frequency ω is assumed to approach the structure from an angle θ measured from the X-axis as shown in Fig. 1. Thereafter, the uni-directional irregular wave modelled using the Bretschneider wave

spectrum is used to study the performance of the iVF-FB and wave climate surrounding the structure. It is to note that the case study is conducted by taking the sea state of Singapore sea as a reference, i.e., the regular wave frequency ω ranges from 1.0 rad/s to 6.0 rad/s whereas the peak wave period T_p ranges from 3 to 6s.

Both FB and VF are designed as hollow boxes to allow for sufficient buoyancy and their outer hulls are made of thin-shell structures. The buoyancy force in the VF must be sufficient to ensure sufficient restoring moment for continuous pitching motion under surging force. The effective draft of the FB is assumed to be 2 m. It is to be noted that the length of FB is adjusted according to the optimal width of the VF with equal spacing s obtained from the parametric study. Also, the length of the supporting frame is determined according to the optimal length of the VF to allow for the VF to pitch without clashing with the FB. The inputs for the numerical study of the full-scale iVF-FB are summarized in Table 1.

3. Mathematical formulation

3.1 Regular wave analysis

3.1.1 Simple potential theory

Simple potential flow theory is used to model the water domain which assumes that the water is incompressible, inviscid and its flow irrotational. The velocity potential may be written as

$$\Phi(x,y,z,t) = Re\left[\varphi(x,y,z)e^{-i\omega t}\right] \tag{1}$$

where $\varphi(x,y,z)$ is the spatial velocity potential taken as the sum of the diffraction φ_D and radiation φ_R potential (Lee and Newman 2005).

According to the linear potential theory, the velocity potential must satisfy the Laplace equation (Dean and Dalrymple 1991, Faltinsen 1993)

$$\nabla^2\varphi = 0 \tag{2}$$

The velocity potential must also satisfy the boundary conditions on the seabed S_B, free surface S_F, infinite surfaces $S_{\mp\infty}$ and the wetted surface S_W (Faltinsen 1993)

$$\frac{\partial\varphi}{\partial z} = 0 \qquad \text{on the seabed } S_B \tag{3}$$

$$\frac{\partial\varphi}{\partial z} = \frac{\omega^2\varphi}{g} \qquad \text{on the free surface } S_F \tag{4}$$

$$\frac{\partial\varphi}{\partial n} = 0 \qquad \text{on the wetted surface } S_W \tag{5}$$

$$\frac{\partial(\varphi_l)_j}{\partial z} = \begin{cases} -i\omega\cdot n_j & \text{for } l = R \\ 0 & \text{for } l = D \end{cases} \qquad \text{on the wetted surface } S_W \tag{6}$$

here $(n_1, n_2, n_3) = \mathbf{n}$ and $(n_4, n_5, n_6) = \mathbf{x}\times\mathbf{n}$ with $\mathbf{n}$ and $\mathbf{x}$ the unit normal vector and position vector of points on the wetted surface (Lee and Newman 2005), respectively. The subscript $j = 1, 2, 3, 4, 5$ and 6 represents the corresponding normal to the six rigid body motion, i.e., surge, sway, heave, roll, pitch and yaw, respectively. The velocity potential must also satisfy the Sommerfeld boundary condition (Faltinsen 1993)

$$\lim_{|x|\to\infty} \sqrt{|x|}\left(\frac{\partial(\varphi-\varphi_{in})}{\partial|x|} - ik(\varphi-\varphi_{in})\right) = 0 \qquad \text{on the surface at infinity } S_{\pm\infty} \tag{7}$$

where k is the wavenumber, φ_{in} is the velocity potential of the incident wave and $|x| = \sqrt{x^2+y^2}$.

By using Green's 2nd Theorem via free surface Green's function (Brebbia *et al.* 2012), the Laplace equation and the boundary conditions from Eqs. (3) to (7) are transformed into a boundary integral equation (BIE). The wetted surface of iVF-FB is discretized into panels in ANSYS AQWA. The PTO system is modelled as a damper with PTO damping B_{PTO} in AQWA.

3.1.2 Equation of motion of floating body

The iVF-FB is assumed to be a rigid body where the motion $\mathbf{W}(x,y,z,t)$ is oscillating with the wave frequency ω as

$$\mathbf{W}(x,y,z,t) = W(x,y,z)e^{-i\omega t} \tag{8}$$

where $W(x,y,z)$ is the spatial rigid body motion given as

$$W(x,y,z) = \{w_x \quad w_y \quad w_z \quad \vartheta_x \quad \theta_y \quad \vartheta_z\}^T \tag{9}$$

where $\{w_x \quad w_y \quad w_z \quad \vartheta_x \quad \theta_y \quad \vartheta_z\}^T$ are the six rigid-body motions, i.e. the surge, sway, heave, pitch, roll and yaw.

The equation of motion of the floating body written in matrix form is thus given by

$$[-\omega^2(\mathbf{M}+\mathbf{M_a}) - i\omega(\mathbf{B_a}+\mathbf{B_{PTO}}) + \mathbf{K}]\cdot W = \mathbf{F} \tag{10}$$

where $\mathbf{M}$ comprises the mass m and moment of inertia I in the corresponding x-, y- and z-axes, given as, $\mathbf{M} = \text{diag}(m_x \quad m_y \quad m_z \quad I_x \quad I_y \quad I_z)$whereas $\mathbf{M_a}$ and $\mathbf{B_a}$ are, respectively, the 6×6 added mass/inertia and radiated damping correspond to the six degrees of freedom (DOF). The PTO damping B_{PTO} is the damping applied in the local $y-$axis of each VF to convert the pitch motions into electricity. $\mathbf{F} = \{F_x \quad F_y \quad F_z \quad M_x \quad M_y \quad M_z\}^T$ where F_x, F_y and F_z are the exciting forces about the x-, y- and z-axes, respectively whereas M_x, M_y and M_z are the exciting moment (or exciting torque) about the x-, y- and z-axes, respectively. $\mathbf{K} = \text{diag}(k_{Lx} \quad k_{Ly} \quad k_{Lz} \quad k_{Rx} \quad k_{Ry} \quad k_{Rz})$ is the hydrostatic stiffness matrice of the floating bodies, where k_L is the linear hydrostatic stiffness and k_R the rotational hydrostatic stiffness.

The FB is only allowed to heave where its horizontal motions, i.e., sway and surge are constrained. On the other hand, the VF only rotates about the hinge, thereby these assumptions further simplify the equation of motion (10). For the case of the VF, the equation of motion of a single VF about the hinge is given as

$$\left[-\omega^2\left(I_y + I_{ay}\right) - i\omega\left(B_{ay} + B_{pto}\right) + k_{Ry}\right]\vartheta_y = M_y \tag{11}$$

where I_{ay} is the added inertia in the y-axis and B_{ay} the radiated damping in the y-axis.

The rotational motion of the VF depends on the moment of inertia, I_y (Lewandowski 2004) calculated from Eq. (12). As the WEC is hinged at the end of the supporting frame, the reference axis for the VF is taken 0.25m below the top tip of the flap as given in Fig. 2. To obtain the mass moment of inertia, the parallel axis theorem is used at this reference axis as

$$I_y = \frac{1}{12}m(L_{WEC}^2 + t_{WEC}^2) \tag{12}$$

The PTO damping B_{pto} in Eq. (11) is the optimum PTO damping given by Falnes (2002) as

$$B_{pto} = \sqrt{\frac{\left[k_{Ry} - \omega^2 (I - I_{ay})\right]^2}{\omega^2} + {B_{ay}}^2} \tag{13}$$

The B_{pto} value is taken as a constant in the numerical simulation. It is computed from Eq. (13) by taking the largest value of the radiated damping B_{ay} and added inertia I_{ay} generated for each VF, for wave period T ranging from 1s to 60s.

3.1.3 Power absorption

By solving Eq. (11), the pitch response amplitude operator (RAO) of the VF could be used to derive the absorbed power P_a of the n^{th} WEC as follows

$$P_a|_n = \frac{1}{2}\omega^2 \ B_{PTO}|RAO|_n^2 \tag{14}$$

The total absorbed power P_T under regular wave is then given by

$$P_T = \sum_{n=1}^{N} P_a|_n \tag{15}$$

3.1.4 Wave elevation

The ANSYS AQWA also allows the computation of the wave elevation surrounding the floating structure. The wave elevation amplitude η on the water surface surrounding the iVF-FB is computed from Eq. (16) as

$$\eta = \frac{1}{g}\left|\frac{\partial \varphi}{\partial t}\right| \tag{16}$$

where φ is the velocity potential obtained from the BIE and g the gravitational acceleration.

3.2 Irregular wave analysis

The Bretschneider (BS) wave spectrum is used to model the sea condition for irregular waves. It is a two-parameter Pierson Moskowitz spectrum that can be expressed as (Goda 2010),

$$S(\omega) = 5\pi^4 \frac{H_S^2}{T_p^4}\frac{1}{\omega^5}\exp\left[-\frac{20\pi^4}{T_p^4}\frac{1}{\omega^4}\right] \tag{17}$$

where T_p is the peak wave period and H_s the significant wave height.

To obtain the significant absorbed power $(P_a)_S$ of the iVF-FB, the response spectrum $S_R(\omega)$ is first computed using Eq. (18) (Chakrabarti 1994)

$$S_R(\omega)|_n = |P_a(\omega)|_n|^2 \times S(\omega) \tag{18}$$

where $P_a|_n$ is the absorbed power of the n^{th} WEC given in Eq. (15) and $S(\omega)$ the BS wave spectrum given in Eq. (17). The significant absorbed power $(P_a)_S|_n$ for the n^{th} WEC is then computed from

$$(P_a)_S|_n = 2\sqrt{m_0} \tag{19}$$

here m_0 is the square root of the zeroth-order moment given as

$$m_0 = \int_\omega S_R(\omega) \cdot d\omega \tag{20}$$

The total significant absorbed power $(P_a)_S$ for uni-directional irregular wave is then given by

$$(P_T)_S = \sum_n^N (P_a)_S|_n \tag{21}$$

The CWR is commonly used to express the capture efficiency of a WEC and is defined as the ratio of the absorbed power to the power in the width of the wave equal to the width of the device or capture width (Babarit 2015). The capture width ratio CWR of a WEC is given as

$$CWR = \frac{(P_T)_S}{P_{res} \cdot W_{WEC}} \tag{22}$$

where the wave power resources P_{res} is given as (Boccotti 2000)

$$P_{res} = \frac{\rho g^2}{64\pi} H_s^2 T_p \tag{23}$$

where H_s is the significant wave height and T_p the peak wave period.

4. Verification of numerical model

To validate the energy generation mechanism of the present numerical model in generating energy via its rotational motion, the results of an OWSC, which operates with a similar mechanism as the VF, are considered. Both OWSC and VF utilize PTO systems to generate electricity via their pitching motions as waves hit on the structure. The OWSC is however bottom mounted to the seabed as opposed to the VF that is hinged connected to a supporting frame attached to the FB. Nevertheless, the mechanism for both structures is similar where both structures depend significantly on the buoyancy and wave forces of the WECs to achieve continuous pitching motion, i.e., continuous energy generation. To validate the present numerical model, the OWSC given by Renzi *et al.* (2014) is first modelled in ANSYS AQWA. The OWSC is then subjected to a regular wave of wave period $T = 4$s to 14s and its hydrodynamic coefficients are compared with their counterparts presented in the literature. The particulars for the OWSC device are presented in Table 2 (Renzi *et al.* 2014) and the thickness, PTO damping and width of the WEC are taken from Tay and Venugopal (2017a, b, 2019, 2022).

Fig. 3 shows the comparison of the exciting torque and radiated damping of the OWSC generated by the present numerical model with the results obtained from Renzi *et al*. (2014). The results

Table 2 Dimension and properties of OWSC

Properties	OWSC
Thickness (m)	4.0
Width (m)	18.0
Immersion depth (m)	9.4
Water depth (m)	10.9
Mass moment of inertia (kg.m^2)	6.6054 x 10^6
PTO damping (kg.m^{2}s^{-1})	16 x 10^6

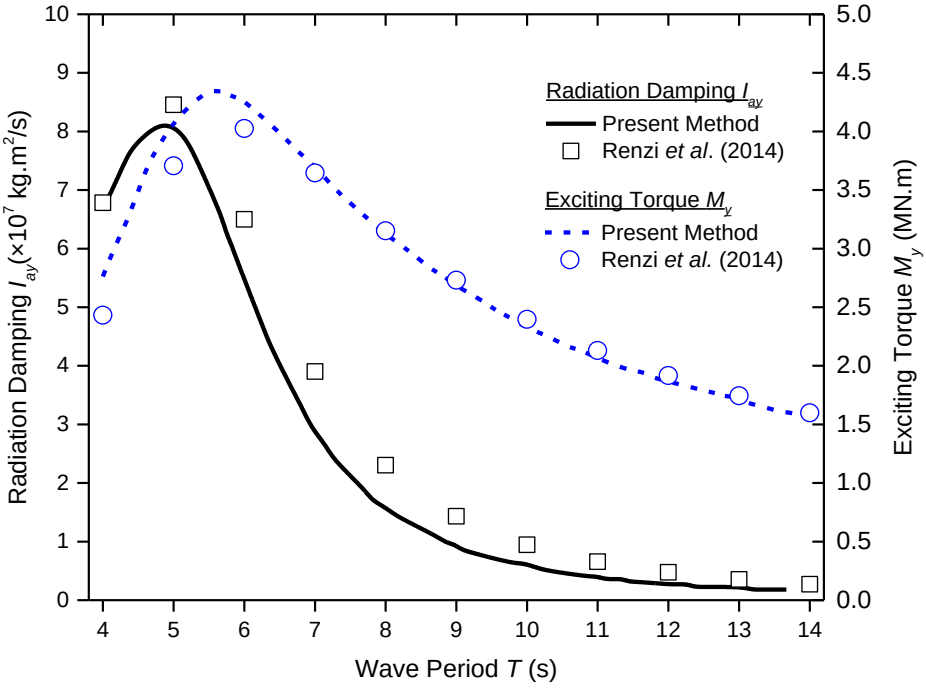

Fig. 3 Validation of radiation damping and exciting torque for Oyster 1 OWSC

predicted by the present numerical model agree well with those published in the literature. The slight discrepancy between the results predicted by the present model with those by Renzi *et al.* (2014) is due to the different modelling methodologies used, where the ANSYS AQWA utilizes the boundary element method that solves the diffracted and radiation waves whereas the latter is based on a semi-analytical method. Nevertheless, the trend of the hydrodynamic coefficients for both models are in good agreement and the difference between the two results is small, thereby validate the energy generation mechanism of the present model.

5. Results and discussion

With the numerical model in ANSYS AQWA validated for its accuracy in energy generation, the iVF-FB is next modelled. The FB and VF are modelled as hollow box-like structures such that only the wetted surfaces of the structure are modelled. The VF is hinged connected to the FB and the PTO systems are modelled as damping in the software. Parametric studies are first conducted on a single VF attached to the FB under regular wave to obtain the optimal dimensions, i.e., length L_{WEC} and width W_{WEC} of the VF. The effect of the motion of the FB has on energy generation is also investigated. Thereafter, the full-scale iVF-FB with 25 VFs is then modelled using the optimal dimensions obtained from the parametric study where the performance and wave attenuation effectiveness is studied. The regular and uni-directional irregular waves are considered with waves arriving from the headsea (0°) and oblique sea (45°).

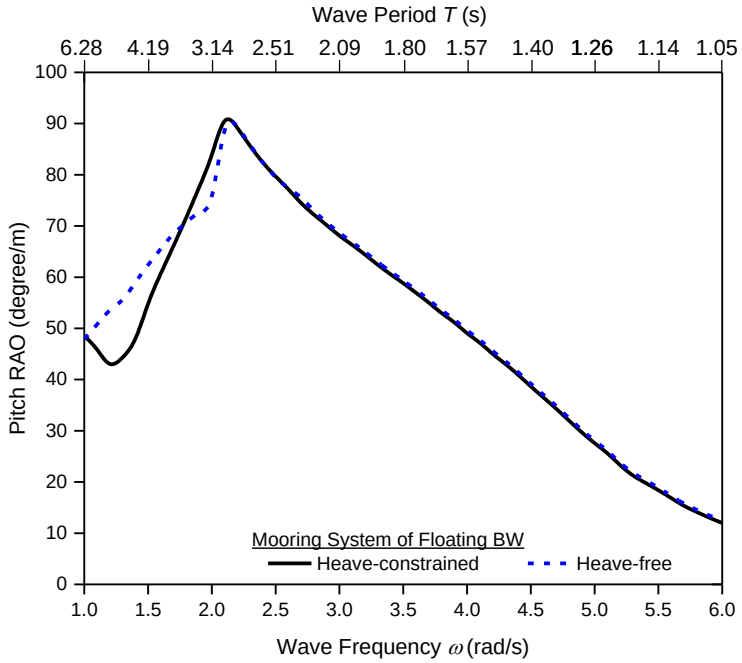

Fig. 4 Pitch RAO for VF when integrated to heave-constrained and heave-free FB. $\boldsymbol{w_{WEC} = 1\ \mathbf{m}}$, $\boldsymbol{L_{WEC} = 1\ \mathbf{m}}$

5.1 Parametric study on single vertical flap

The parametric studies are considered in this section to obtain the optimal VF's dimensions in maximizing the performance of the WEC. The single VF attached to a FB is considered under regular waves. The effect of the mooring system of the floating breakwater, width and length of the WECs has on the performance of the WEC is presented hereafter.

5.1.1 Effect of motion of floating breakwater

The effect of motion of the FB is first investigated. The box-like FB as shown in Fig. 1 is moored by mooring line by assuming that only the heave motion of the FB is allowed. In this analysis, the energy generation from the iVF-FB when the FB is free to heave (termed heave-free) is compared with its counterpart when it is heave-constrained. The heave-constraint is imposed in ANSYS AQWA by imposing fixed motion to the heave DOF. This is analogous to having the FB moored by mooring lines with very high stiffness. The pitch RAO of the single VF when it is hinged to the heave-constrained and heave-free FBs is shown in Fig. 4. The length and width of the VF are $L_{WEC} = W_{WEC} = 1$ m. The result shows that the effect of the motion of the FB is negligible towards the pitch RAO when subjected to regular waves of high frequency. While the integrated VF with heave-free FB shows a slightly greater pitch RAO at a low frequency between 1.0 rad/s to 1.7 rad/s, the heave-constraint FB results in a higher pitch RAO for a wave frequency between 1.7 rad/s to 2.0 rad/s, i.e., wave period $T \sim 3$ to 4s, which is close to a typical tropical sea state in Singapore. This is

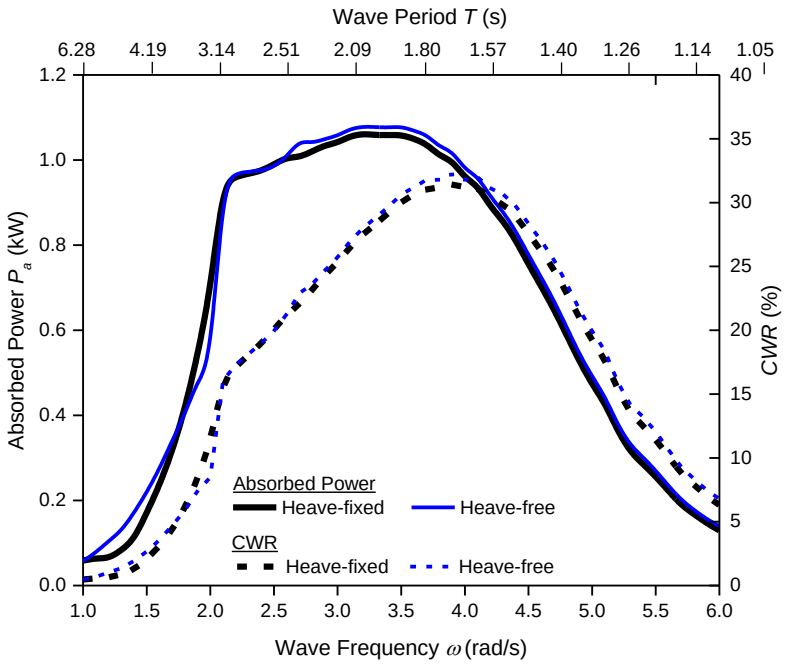

Fig. 5 Absorbed power for single VF when integrated to heave-constrained and heave-free FB. $\boldsymbol{w_{WEC} = 1\ \mathbf{m}}$, $\boldsymbol{L_{WEC} = 1\ \mathbf{m}}$, $\boldsymbol{B_{PTO} = 164}$ Nms/rad

in agreement with the results published by Tay (2020) where it was reported that the heave-constrained FB allows the greater energy generation from a raft-type WEC due to the greater relative pitching motion when attached to a heave-constrained FB. Figure 4 also shows that the pitch RAO of the VF reduces with the increase of wave frequency. This is because the wavelength is short at high frequency thus results in smaller wave energy resources. The pitch RAO is also found to peak when the wave frequency is around 2.0 rad/s, which coincides with the most occurrence sea state of the Singapore sea which is around T~2 to 4s.

Fig. 5 shows the absorbed power P_a and CWR of the single VF with $L_{WEC} = W_{WEC} = 1$m when subjected to regular wave. P_a is represented by the solid line (──) whereas the CWR by the broken line (----). The absorbed power is found to increase with the increase of the wave frequency ω and maintains an almost constant peak power absorption when the wave frequency is around ω~2.0 to 3.5rad/s, corresponding to the wave period T~2 to 3s. The P_a then reduces with the increase in wave frequencies due to the short wavelength, i.e., smaller wave energy resource. Fig. 5 also shows that the single VF can achieve CWR above 15% for a range of wave frequency between 2.0 to 5.0 rad/s, and reaches a peak of 30% at $\omega = 4.0$rad/s. The comparison of the performance of the VF with heave-free and heave-constrained FB shows that the motion of the FB does not significantly affect the power absorption and CWR of the WEC. However, the heave-constrained FB shall be taken in the subsequent analyses due to its relatively better performance when operating in the sea condition of the tropical sea, by taking Singapore as a case study. A FB with minimal motion is important to ensure the safety and comfortability of the crew working on the structure. Also, a FB with smaller motion generates lesser radiated waves under wave action.

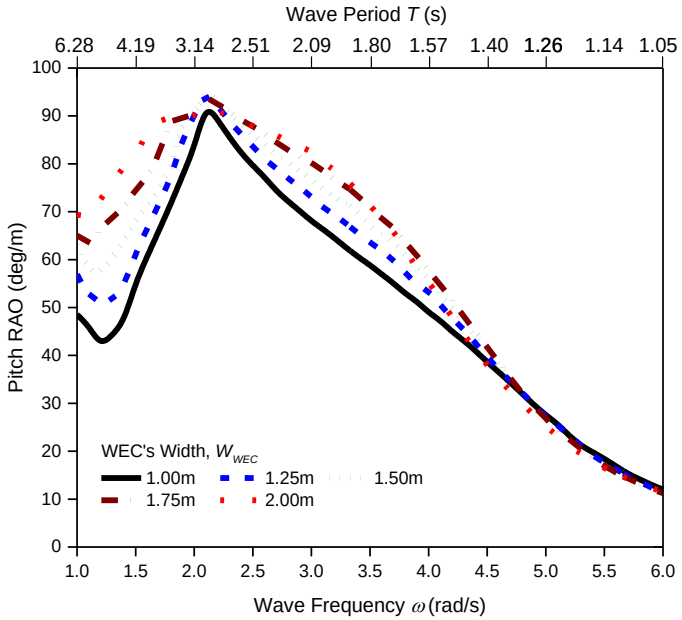

Fig. 6 Pitch RAO for single iVF-FB with different width $\boldsymbol{W_{WEC}}$. $\boldsymbol{L_{WEC} = 1\ m}$, heave-constrained FB

5.1.2 Effect of width of WEC

By assuming a heave-constrained FB, five different VF with varying widths, i.e., $W_{WEC} = 1.00\ \text{m}, 1.25\ \text{m}, 1.50\ \text{m}, 1.75\ \text{m}$ and $2.00\ \text{m}$, are considered to study the effect the width has on the power generation of the WEC. The pitch RAO of the five different VF, when attached to the heave-constrained FB under headsea condition, is presented in Fig. 6. The length of the VF is taken to be $L_{WEC} = 1.00\ \text{m}$. Fig. 6 shows that the pitch RAO for all the considered VFs has the same trend as the VF with $W_{WEC} = 1.00\ \text{m}$ considered in Fig. 4, i.e., the pitch RAO increases with ω and decreases after reaching a peak at $\omega = 2.0\text{rad/s}$. It can be seen that the pitch RAO increases significantly with the increase in the width of the WEC with $W_{WEC} = 2.00\ \text{m}$ producing a relatively larger pitching motion for all the wave frequencies considered. It is to note that the peak pitch RAO is about 90 degree/m indicating that the VF can swipe a wide-angle of 45° from its vertical neutral position (see Fig. 2) as the wave hits on the structure.

By computing the power absorbed P_a from Eq. (14), the P_a is plotted in Fig. 7(a). It is noted that P_a obtained from Eq. (14) depends on the B_{PTO} which differs for different geometries of the VF (varying W_{WEC} and L_{WEC}). This is because the optimal B_{PTO} is computed from Eq. (13) that depends on the added inertia I_a, radiated damping B_a and hydrostatic stiffness k_{Ry} which are different for VF of different geometries. The corresponding optimal B_{PTO} for the VF with different W_{WEC} is labelled in Fig. 7(a). It shows that the B_{PTO} is the largest for VF with $W_{WEC} = 1.25\ \text{m}$. The value of B_{PTO} has a profound effect on the power absorption as shown in Fig. 7(a), where the largest P_a is produced by the VF with $W_{WEC} = 1.25\ \text{m}$. It is interesting to see that VF with $W_{WEC} = 2.00\ \text{m}$ generates the smallest P_a due to the small optimal $B_{PTO} = 64$ N.m.s/rad even though its pitch RAO is the highest as shown in Fig. 6. Fig. 7(a) shows that the P_a increases as the W_{WEC} increases from 1.00 m to 1.50 m with W_{WEC} =1.25 m generating the highest power.

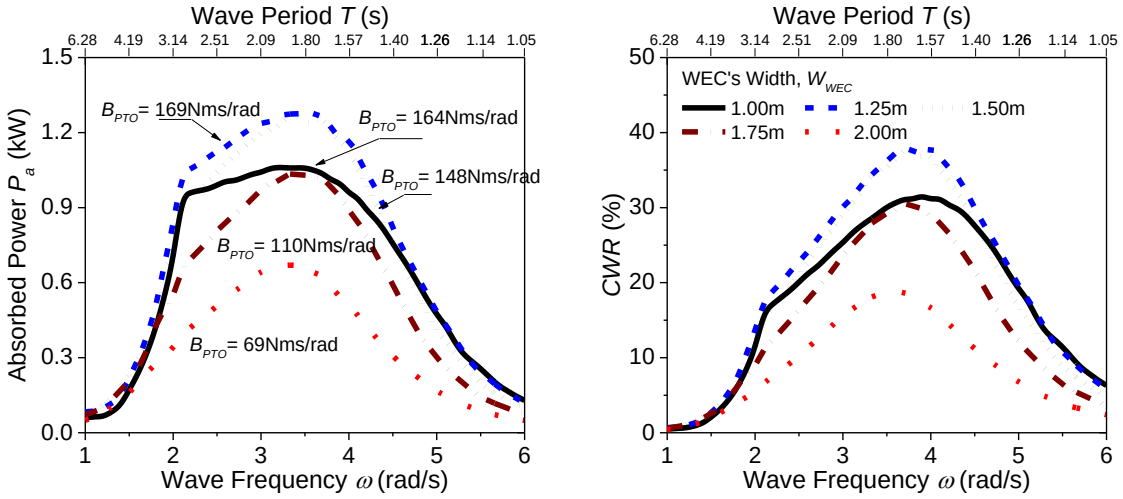

(a) (b)

Fig. 7 (a) Absorbed power P_a and (b) CWR, for single iVF-FB with varying width W_{WEc}. L_{WEC} = 1.00 m, heave-constrained FB

However, the power generated significantly decreases for W_{WEC} larger than 1.50 m. This phenomenon can be explained by referring to the effect of B_{PTO} where it can be seen from Fig. 7(a) that the optimal B_{PTO} for $W_{WEC} \leq 1.50$ m is larger than its counterpart for $W_{WEC} > 1.50$ m, thus generating more energy according to Eq. (14).

In the parametric study to investigate the effect of W_{WEC}, Fig. 7(b) shows that under optimal $W_{WEC} = 1.25$m, a CWR up to 40% could be achieved at $\omega = 4.0$ rad/s and the CWR is above 20% for wave frequency ranging from 2.0rad/s to 5.0 rad/s, i.e., higher than the CWR presented in Fig. 5, thereby suggesting a wider bandwidth for VF with $W_{WEC} = 1.25$ m could be achieved.

5.1.3 Effect of length of WEC

In this section, the effect of L_{WEC} has on the pitch motion, power absorption and CWR is studied when the $W_{WEC} = 1.25$ m and FB is heave-constrained. Five different L_{WEC} are considered, i.e., $L_{WEC} = 1.00$ m, 1.25 m, 1.50 m, 1.75 m and 2.00 m. The pitch RAO is first presented in Fig. 8 for the varying L_{WEC} where the pitch RAO is found to increase with the decrease of the L_{WEC}. This phenomenon can be explained by referring to the moment of inertia of the VF where a shorter VF has a smaller I_y as compared to the longer VF. As a result, the VF with a smaller I_y pitches with a larger Θ_y and therefore the Θ_y for the largest $L_{WEC} = 2.00$ m is significantly small as shown in Fig. 8.

Similar to the effect of varying W_{WEC} studied in Fig. 7(a), the power absorption also depends on the optimal B_{PTO} of the VF, which varies for VF with different L_{WEC}. The P_a of the VF with varying L_{WEC} is plotted in Fig. 9(a). Fig. 9(a) shows that the effect of length has a greater influence compared to the width of the VF (plotted in Fig. 7a) where the P_a differs with a larger magnitude for varying L_{WEC} as compared to the influence of varying W_{WEC}. Also, when keeping the WEC width at its optimal value of $W_{WEC} = 1.25$ m, Fig. 9(a) shows that the P_a of the VF could be further increased by increasing the L_{WEC} where the P_a for $L_{WEC} = 2.00$ m is twice the value

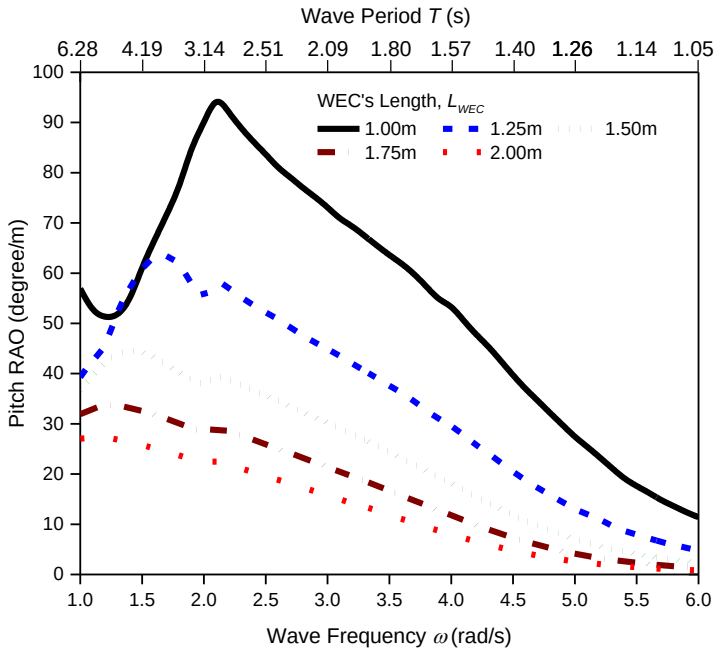

Fig. 8 Pitch RAO for single iVF-FB with different length $\boldsymbol{L_{WEC}}$. $\boldsymbol{W_{WEC}} = \mathbf{1.25}$ m, heave-constrained FB

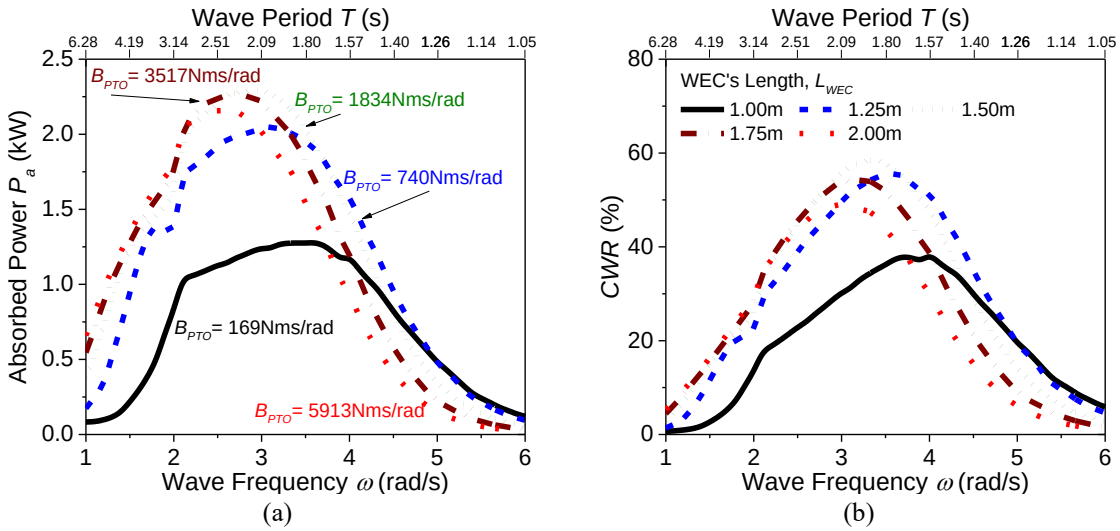

Fig. 9 (a) Absorbed power P_a and (b) CWR, for single iVF-FB with different L_{WEC}. $W_{WEC} =$ 1.25 m, heave-constrained FB. Note: Legend and B_{PTO} are the same for Figs. 9(a) and (b)

when $L_{WEC} = 1.00$ m as considered in Fig. 7(a). It is to note that $L_{WEC} = 2.00$m is taken as the optimal length even though the P_a drops when the ω is greater than 2.5 rad/s. This is because the maximum power absorption occurs when the VF is operating at $\omega \leq 2.5$ rad/s, which is the typical sea state of the Singapore sea. The CWR of the VF for varying L_{WEC} is also given in Fig. 9(b)

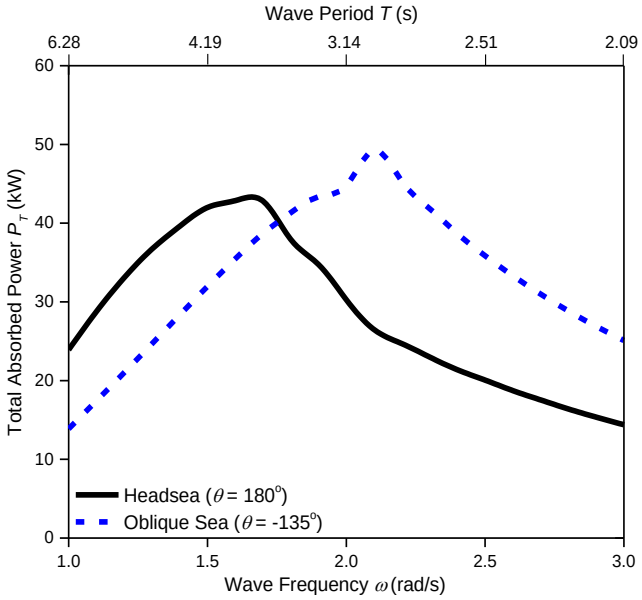

Fig. 10 Total absorbed power of full-scale iVF-FB ($\boldsymbol{N_{WEC} = 25}$) under headsea and oblique sea conditions. Regular waves. $\boldsymbol{W_{WEC} = 1.25}$ **m**, $\boldsymbol{L_{WEC} = 2.00}$ **m**, $\boldsymbol{B_{PTO} = 5913}$ **Nms/rad**, heave-constrained FB

where it can be seen that the CWR is greater than 20% for ω ranging from 2.0 rad/s to 5.0 rad/s and maximum $CWR = 60\%$. The overall energy absorption bandwidth increases with the increase of L_{WEC}.

5.2 Fully integrated FB-WEC under regular wave

In this section, a full-scale iVF-FB is considered, where 25 VFs with optimal $W_{WEC} = 1.25$ m and $L_{WEC} = 2.00$ m are hinged connected to the 50m heave-constrained FB. The B_{PTO} is 5,913 Nms/rad taken from Fig. 9 for $L_{WEC} = 2.00$m. The iVF-FB is subjected to regular and irregular waves under headsea and oblique sea to study the power generation of the VF and wave attenuation effectiveness of the FB. The total absorbed power P_T of the 25 VFs under the headsea and oblique sea, obtained from Eq. (15), is presented in Fig. 10. It is noted that only the most occurrence wave frequencies ranging from 1.0rad/s to 3.0rad/s (corresponds to $T =$ 2 to 6s) are considered in Fig. 10.

Fig. 10 shows that the iVF-FB has a wide energy generation bandwidth where it can generate a substantial amount of energy for a wide range of frequencies. The iVF-FB under headsea is more effective at smaller wave frequency, i.e., $\omega \leq 1.75$rad/s whereas iVF-FB under the oblique sea could generate more energy at $\omega > 1.75$rad/s. The largest P_T occurs when the wave period is between $T =$ 2 to 4s.

The effectiveness of the iVF-FB in attenuating the wave force is next investigated. Figs. 11 and 12 show the wave climate surrounding the iVF-FB under headsea and oblique sea, respectively. Four different wave periods are considered, i.e. $T =$ 3s, 4s, 5s and 6s and plotted in the sub-figure (a),

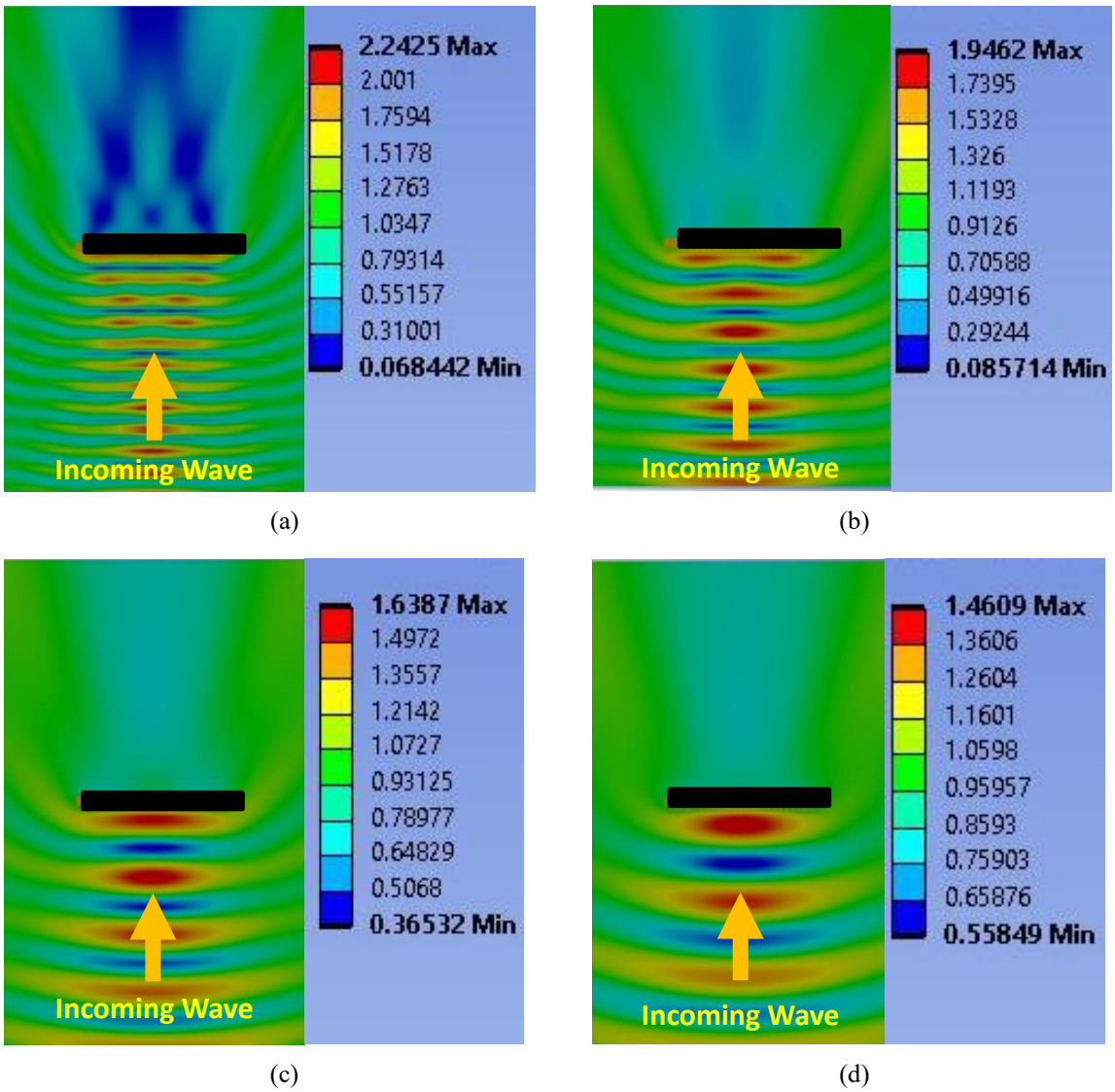

Fig. 11 Wave elevation amplitude surrounding full-scale iVF-FB for wave period (a) $T = 3s, \lambda/W_{FB} = 4.68$ (b) $T = 4s, \lambda/W_{FB} = 8.23$ (c) $T = 5s, \lambda/W_{FB} = 12.20$ (d) $T = 6s, \lambda/W_{FB} = 16.14$. Headsea. $W_{WEC} = 1.25$ m, $L_{WEC} = 2.00$ m, $B_{PTO} = 5913$ Nms/rad, heave-constrained FB.

(b), (c) and (d), respectively, of Figs. 11 and 12. Figs.11 and 12 show that the FB is very effective in attenuating the wave force when the wavelength is small, i.e., T =3s where the wave amplitude downstream of the FB is negligibly small. This is due to the relatively small wavelength to FB width ratio, i.e., $\lambda/W_{FB} = 4.68$ as compared to its counterpart with higher λ/W_{FB}. This also implies that the effectiveness of the FB depends significantly on the width of the FB. The wave upstream of the iVF-FB is found to be higher when the wavelength is small, due to the greater inferences between the incoming and reflected waves.

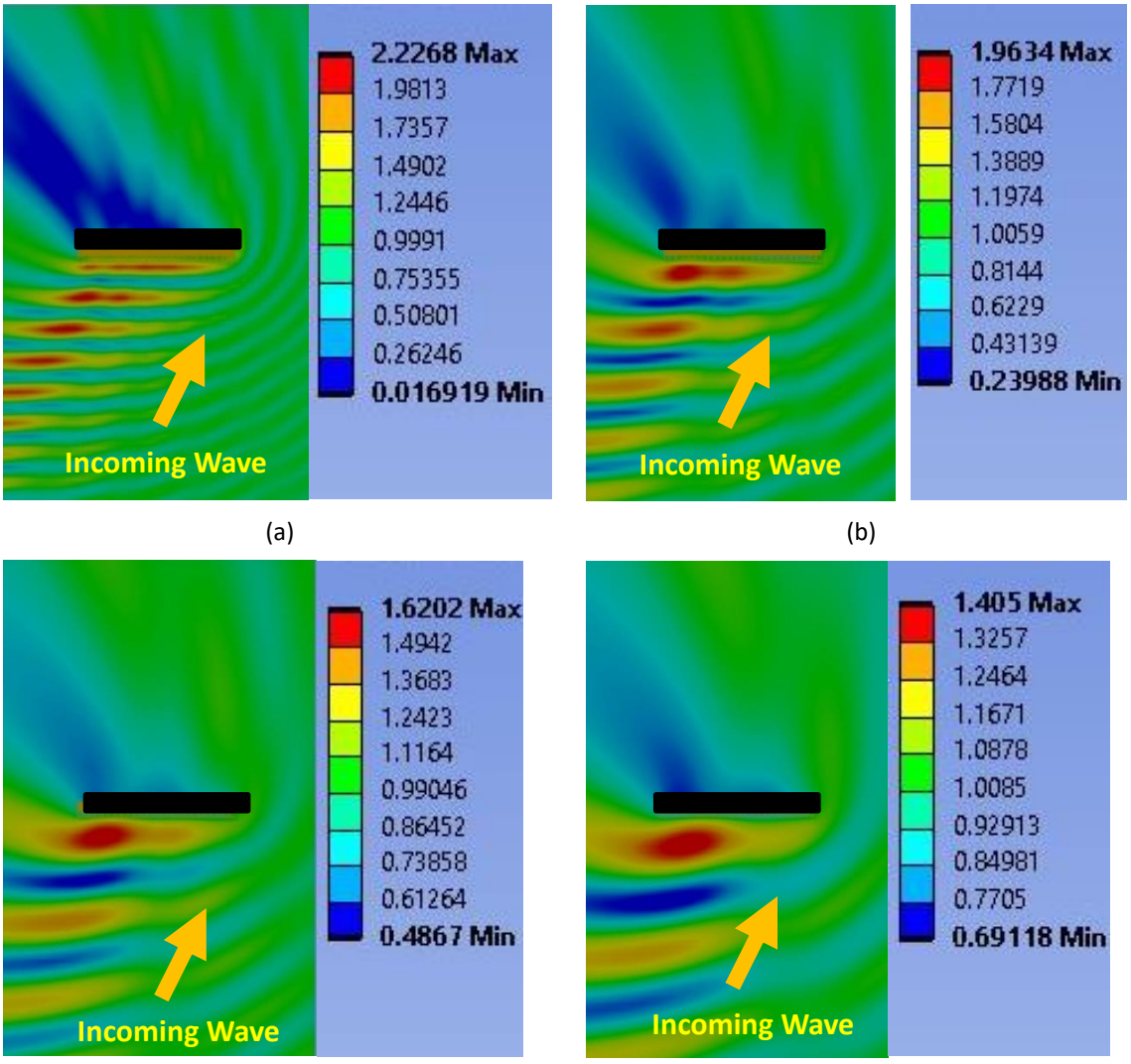

Fig. 12 Wave elevation amplitude surrounding full-scale iVF-FB for wave period (a) $T = 3s, \lambda/W_{FB} = 4.68$ (b) $T = 4\text{s}, \lambda/W_{FB} = 8.23$ (c) $T = 5s, \lambda/W_{FB} = 12.20$ (d) $T = 6s,\ \lambda/W_{FB} = 16.14$. Oblique sea ($\theta = 45°$). $W_{WEC} = 1.25$ m, $L_{WEC} = 2.00$ m, $B_{PTO} = 5913$ Nms/rad, heave-constrained FB

5.3 Fully integrated FB-WEC under uni-directional Irregular wave

The performance of the iVF-FB in terms of power generation under irregular waves is next studied. The Bretschneider (BS) wave spectrum given in Eq. (17) is used to model the uni-directional waves, by taking the significant wave height as $H_S = 2\text{m}$ and peak wave period T_p ranging from 3s to 6s, with an interval of 1s. The BS wave spectrum for the different T_p is plotted in Fig. 13.

The total significant absorbed power $(P_T)_S$ for the headsea and oblique sea are presented in Figs. 14 and 15, respectively. Fig. 14 shows that the $S_R(\omega)$ is larger when the wave frequency is

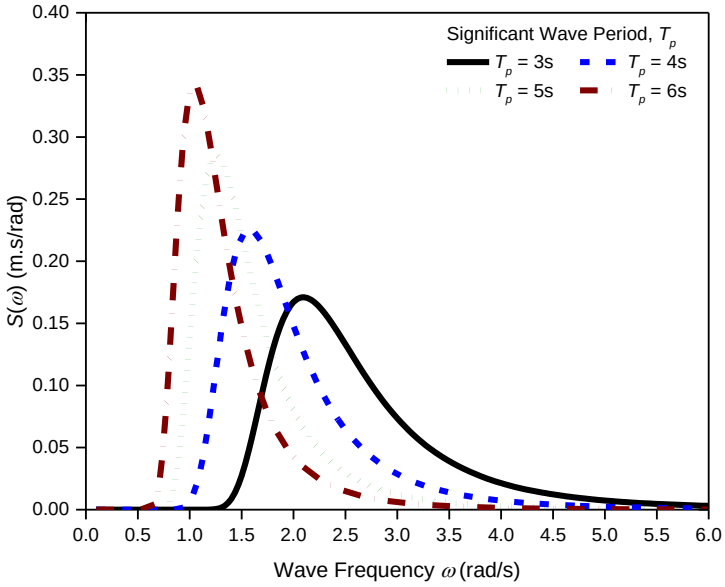

Fig. 13 Bretschneider wave spectrum for peak wave period $\mathbf{T_p = 3s}$, 4s, 5s and 6s. $\mathbf{H_s = 3}$ m

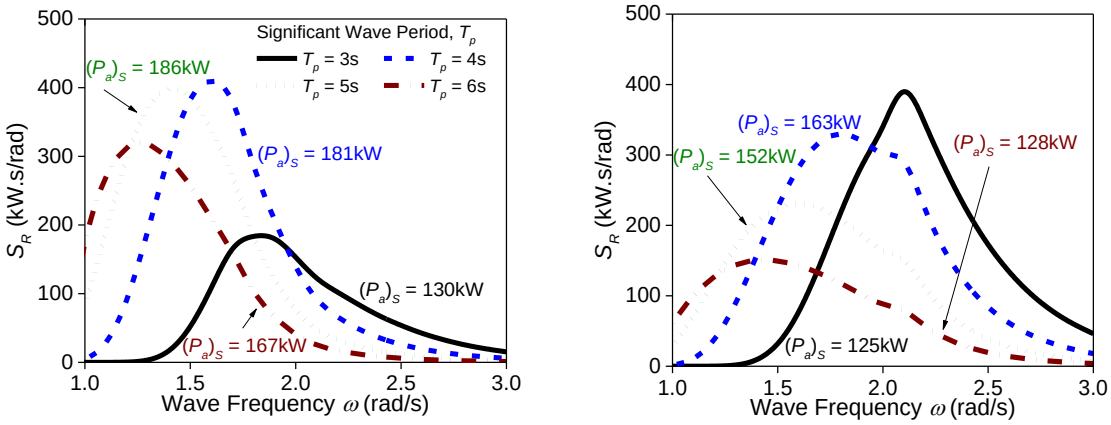

(a) (b)

Fig. 14 Power response spectrum S_R for full-scale iVF-FB subjected to irregular wave under (a) headsea (b) oblique sea. $H_s = 3$ m. $W_{WEC} = 1.25$ m, $L_{WEC} = 2.00$, $B_{PTO} = 5{,}913$ Nms/rad, heave-constrained FB

small, which agrees with the finding on the total absorbed power P_T (under regular wave) presented in Fig. 10 where the P_T has a greater value when the $\omega \leq 1.75$s (i.e., $T \geq 3.6$s) and gradually reduce when $\omega > 1.75$rad/s (i.e., $T < 3.6$s). The iVF-FB under headsea has the highest $(P_T)_S$ when subjected to irregular waves with $T_p = 4$s and 5s. It is to note that, although the $(P_T)_S$ is the smallest under $T_p = 3$s, the amount of energy generated is substantially high, i.e., $(P_T)_s = 130$kW.

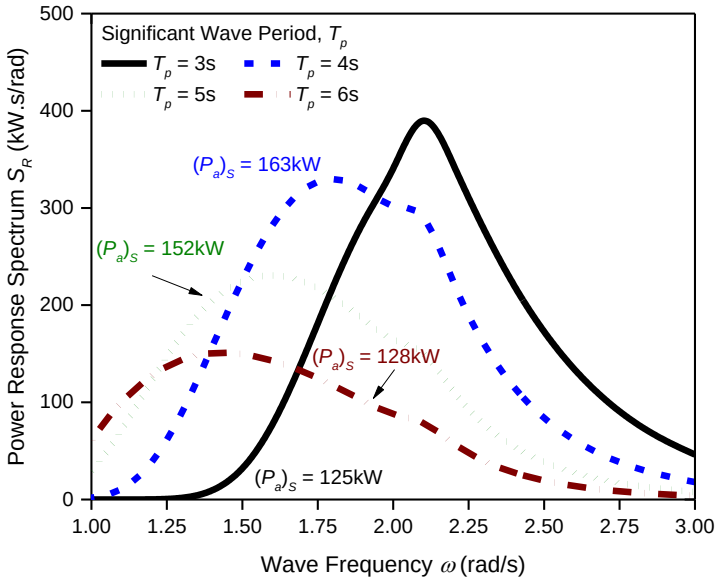

Fig. 15 Power response spectrum $\boldsymbol{S_R(\omega)}$ for full-scale iVF-FB under varying peak wave $\boldsymbol{T_p}$. Oblique sea ($\boldsymbol{\theta = 45°}$), $\boldsymbol{H_S = 2\ m}$. $\boldsymbol{W_{WEC} = 1.25\ m}$, $\boldsymbol{L_{WEC} = 2.00}$m, $\boldsymbol{B_{PTO} = 5913\ Nms/rad}$, heave-constrained FB

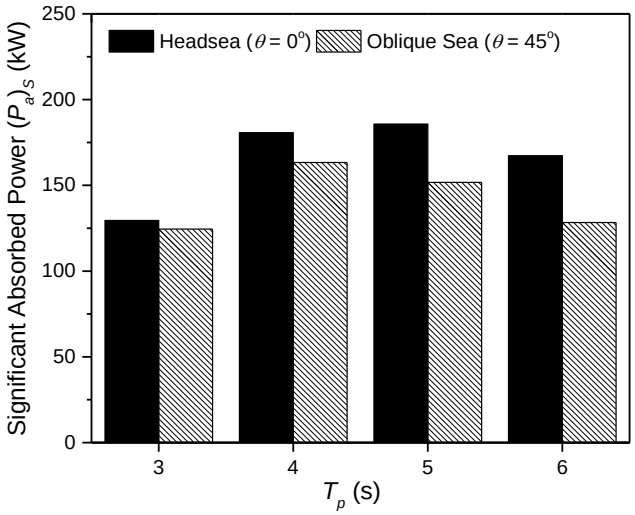

Fig. 16 The significant power of full-scale iVF-FB under irregular waves. $\boldsymbol{H_S = 2\ m}$. $\boldsymbol{W_{WEC} = 1.25\ m}$, $\boldsymbol{L_{WEC} = 2.00}$ m, $\boldsymbol{B_{PTO} = 5913\ Nms/rad}$, heave-constrained FB

The response spectrum $S_R(\omega)$ under the oblique sea, as plotted in Fig. 15 has a different trend as compared to the headsea. It can be seen that the iVF-FB generates the most energy when $T_p =$ 3s, influenced significantly by the behaviour of the P_T (see Fig. 10) where P_T is the largest when $\omega \approx 2.0$ rad/s (i.e., 3.1s) and gradually decreases when $\omega < 2.0$ rad/s and $\omega > 2.0$ rad/s. A

comparison between Figs. 14 and 15 shows that the iVF-FB is most effective in energy generation when the T_p is 4s, which falls in the range of the most occurrence significant peak wave periods of the Singapore sea.

The total significant absorbed power $(P_T)_S$ for the headsea and oblique sea is summarised in Fig. 16. It can be seen that the iVF-FB produces more energy when waves approach from the headsea but the difference between the headsea and oblique is not significant. Also, the overall largest $(P_T)_S$ occurs when $T_p =$ 4s. The $(P_T)_S$ for all T_p is substantially large, i.e., $(P_T)_S > 100$kW implying that the iVF-FB has a wide absorption bandwidth from $T_p =$ 3s to 6s.

6. Conclusions

In the present work, a novel VF integrated with FB, termed the iVF-FB, was proposed. The effectiveness of the iVF-FB for converting wave energy and attenuating wave force was investigated using the numerical software ANSYS AQWA. Two performances indices, i.e., power absorption and wave elevation amplitude were used to assess the performance of the iVF-FB. The key findings of the present work are summarized below:

Motion of FB

The effect of the motion of the FB, whether it is heave-free or heave-constrained is minimal on the power absorption and CWR of the VF. The heave-constrained FB was found to have a slightly higher power absorption at wave frequencies of a typical tropical sea condition ranging from ω =1.7 rad/s to 2.0 rad/s.

Width of WEC

The power absorption from the single VF was found to be the highest for VF with $W_{WEC} = 1.25$ m when the length of the WEC is kept constant at $L_{WEC} = 1.00$ m. The overall wave absorption bandwidth of the VF was found to increase when the VF with optimal $W_{WEC} = 1.25$ m was considered. The maximum CWR is 40% and the CWR is above 20% for ω ranging from 2.0rad/s to 5.0 rad/s

Length of WEC

The power absorption of the VF is significantly affected by L_{WEC} as compared to the W_{WEC} and motion of the FB. The optimal length of the VF is $L_{WEC} = 2.00$ m where the maximum CWR is up to 60% and the CWR is greater than 20% for ω ranging from 2.0 rad/s to 5.0 rad/s

Full-scale iVF-FB

The full-scale iVF-FB, with 25 VFs ($W_{WEC} = 1.25$ m and $L_{WEC} = 2.00$ m, $B_{PTO} = 5{,}913$ Nms/rad) attached to a 50-meter heave-constrained FB, under regular wave has the maximum total power P_T when the wave period $T = 2$s to 4s. The iVF-FB was found to have a high power absorption when subjected to uni-direction irregular waves with T_p of

around 4s which is the typical sea state of Singapore sea. The iVF-FB was also found to be very effective in attenuating the wave force, especially when the wavelength is small.

Acknowledgements

The authors are grateful to the resources provided by the MOE-SIT Strategic Initiative Grant (F-MOE-A204-G005).

References

ANSYS Inc (2012), *AQWA Reference Manual*, ANSYS, Inc, Canonsburg, Pennsylvania, USA.

Astariz, S. and Iglesias, G. (2015), "The economics of wave energy: A review", *Renew. Sust.Energ. Rev.*, **45**, 397-408, https://doi.org/10.1016/j.rser.2015.01.061.

Babarit, A. (2015), "A database of capture width ratio of wave energy converters", *Renew. Energ.*, **80**, 610-628, https://doi.org/10.1016/j.renene.2015.02.049.

Boccotti, P. (2000), *Wave mechanics for ocean engineering*, Elsevier Science, The Netherlands.

Brebbia, C.A., Telles, J.C.F. and Wrobel, L.C. (2012), *Boundary element techniques: theory and applications in engineering*, Springer Science & Business Media.

Cabral, T., Clemente, D., Rosa-Santos, P., Taveira-Pinto, F., Morais, T., Belga, F. and Cestaro, H. (2020), "Performance assessment of a hybrid wave energy converter integrated into a harbor breakwater", *Energies,* **13**(1), 236, https://doi.org/10.3390/en13010236.

Chakrabarti, S.K. (1994), *Offshore structure modeling*, World Scientific, Singapore.

Chen, M., Xiao, P., Zhang, Z., Sun, L. and Li, F. (2021), "Effects of the end-stop mechanism on the nonlinear dynamics and power generation of a point absorber in regular waves", *Ocean Eng*., **242**, 110123, https://doi.org/10.1016/j.oceaneng.2021.110123.

Chum, H.L. and Overend, R.P. (2001), "Biomass and renewable fuels", *Fuel Process. Technol.*, **71**(1-3), 187-195, https://doi.org/10.1016/S0378-3820(01)00146-1.

Dean, R.G. and Dalrymple, R.A. (1991), *Water wave mechanics for engineers and scientists*, World Scientific Publishing Company, Singapore.

Drimer, N., Agnon, Y. and Stiassnie, M. (1992), "A simplified analytical model for a floating breakwater in water of finite depth", *Appl. Ocean Res.*, **14**(1), 33-41, https://doi.org/10.1016/0141-1187(92)90005-5.

Falnes, J. (2002), *Ocean waves and oscillating systems: linear interactions including wave-energy extraction*, Cambridge University Press, UK.

Falnes, J. (2007), "A review of wave-energy extraction", *Mar. Struct*., **20**(4), 185-201, https://doi.org/10.1243/09576509JPE782.

Faltinsen, O. (1993), *Sea loads on ships and offshore structures*, Cambridge university press, UK.

Favaretto, C., Martinelli, L., Ruol, P. and Cortellazzo, G. (2017), "Investigation on possible layouts of a catamaran floating breakwater behind a wave energy converter", *Proceedings of the 27th International Ocean and Polar Engineering Conference*, San Francisco, California, USA, June 2017.

Goda, Y. (2010), *Random seas and design of maritime structures*, World Scientific Publishing Company, Singapore.

He, F., Huang, Z. and Law, A.W.K. (2013), "An experimental study of a floating breakwater with asymmetric pneumatic chambers for wave energy extraction", *Appl. Energ*., **106**, 222-231, https://doi.org/10.1016/j.apenergy.2013.01.013.

Headland, J.R., Alfageme, S., Smith, E. and Kotulak, P. (2007), "Coastal structure design for shore protection and sand retention: practical aspects", *Coastal Sediments' 07*, 2432-2445, https://doi.org/10.1061/40926(239)191.

Herbert, G.J., Iniyan, S., Sreevalsan, E. and Rajapandian, S. (2007), "A review of wind energy technologies", *Renew. Sust.Energ. Rev.*, **11**(6), 1117-1145, https://doi.org/10.1016/j.rser.2005.08.004.

Hornsey, W., Carley, J., Coghlan, I. and Cox, R. (2011), "Geotextile sand container shoreline protection systems: Design and application", *Geotext. Geomembranes*, **29**(4), 425-439, https://doi.org/10.1016/j.geotexmem.2011.01.009.

Howe, D., Nader, J.-R. and Macfarlane, G. (2020a), "Experimental investigation of multiple oscillating water column wave energy converters integrated in a floating breakwater: energy extraction performance", *Applied Ocean Research,* **97**, 102086, 10.1016/j.apor.2020.102086.

Howe, D., Nader, J.-R. and Macfarlane, G. (2020b), "Performance analysis of a floating breakwater integrated with multiple oscillating water column wave energy converters in regular and irregular seas", *Appl. Ocean Res.*, **99**, 102147, https://doi.org/10.1016/j.apor.2020.102147.

Kweku, D.W., Bismark, O., Maxwell, A., Desmond, K.A., Danso, K.B., Oti-Mensah, E.A., Quachie, A.T. and Adormaa, B.B. (2017), "Greenhouse effect: Greenhouse gases and their impact on global warming", *J. Scientific Res. Reports*, 1-9, 10.9734/JSRR/2017/39630.

Lee, C.H. and Newman, J. (2005), "Computation of wave effects using the panel method", *WIT Transactions on State-of-the-art in Science and Engineering*, **18**, 211-251, 10.2495/978-1-85312-837-0/06.

Lewandowski, E.M. (2004), *The dynamics of marine craft: maneuvering and seakeeping*, World scientific Publishing Company, Singapore.

Martinelli, L., Ruol, P. and Favaretto, C. (2016), "Hybrid structure combining a wave energy converter and a floating breakwater", *Proceedings of the 26th International Ocean and Polar Engineering Conference,* Rhodes, Greece, June 2016.

McCartney, B. (1985), "Floating breakwater design", *J. Waterway, Port Coast.Ocean Eng*., **111**(2), 304-318, https://doi.org/10.1061/(ASCE)0733-950X(1985)111:2(304).

Nguyen, H.P. and Wang, C.M. (2020), "Oscillating wave surge converter-type attachment for extracting wave energy while reducing hydroelastic responses of very large floating structures", *J. Offshore Mech. Arct. Eng.*, **142**(4), OMAE-19-1190, https://doi.org/10.1115/1.4045916.

Ning, D., Zhao, X., Göteman, M. and Kang, H. (2016), "Hydrodynamic performance of a pile-restrained WEC-type floating breakwater: An experimental study", *Renew. Energ*., **95**, 531-541, https://doi.org/10.1016/j.renene.2016.04.057.

Owusu, P.A. and Asumadu-Sarkodie, S. (2016), "A review of renewable energy sources, sustainability issues and climate change mitigation", *Cogent Eng*., **3**(1), 1167990, https://doi.org/10.1080/23311916.2016.1167990.

Pilarczyk, K.W. and Press, C. (1990), *Coastal protection*, AA Balkema Rotterdam, The Netherlands.

Quaschning, V.V. (2019), *Renewable energy and climate change*, John Wiley & Sons, New Jersey, USA.

Quirapas, M.A.J.R., Lin, H., Abundo, M.L.S., Brahim, S. and Santos, D. (2015), "Ocean renewable energy in Southeast Asia: A review", *Renew. Sust.Energ. Rev.*, **41**, 799-817, https://doi.org/10.1016/j.rser.2014.08.016.

Renzi, E., Doherty, K., Henry, A. and Dias, F. (2014), "How does Oyster work? The simple interpretation of Oyster mathematics", *Eur. J. Mech.-B/Fluid.*, **47**, 124-131, https://doi.org/10.1016/j.euromechflu.2014.03.007.

Schoonees, T., Mancheño, A.G., Scheres, B., Bouma, T.J., Silva, R., Schlurmann, T. and Schüttrumpf, H. (2019), "Hard structures for coastal protection, towards greener designs", *Estuaries and Coasts,* **42**(7), 1709-1729, https://doi.org/10.1007/s12237-019-00551-z.

Shin, E. and Oh, Y. (2007), "Coastal erosion prevention by geotextile tube technology", *Geotext. Geomembranes,* **25**(4-5), 264-277. https://doi.org/10.1016/j.geotexmem.2007.02.003.

Shine, K.P., Fuglestvedt, J.S., Hailemariam, K. and Stuber, N. (2005), "Alternatives to the global warming potential for comparing climate impacts of emissions of greenhouse gases", *Climatic Change*, **68**(3), 281-302, 10.1007/s10584-005-1146-9.

Tay, Z.Y. (2017), "Energy generation from anti-motion device of very large floating structure", *Proceedings of the Twelfth European Wave and Tidal Energy Conference*, 27 August 2017 - 1 September 2017, Cork, Ireland 674-1.

Tay, Z.Y. (2019), "Energy extraction from an articulated plate anti-motion device of a very large floating structure under irregular waves", *Renew. Energ.,* **130**, 206-222, https://doi.org/10.1016/j.renene.2018.06.044.
Tay, Z.Y. (2020), "Performance and wave impact of an integrated multi-raft wave energy converter with floating breakwater for tropical climate", *Ocean Eng*., **218**, 108136, https://doi.org/10.1016/j.oceaneng.2020.108136.
Tay, Z.Y. (2021), "Effect of resonance and wave reflection in semi-enclosed moonpool on performance enhancement of point absorber arrays", *Ocean Eng*., 110182, https://doi.org/10.1016/j.oceaneng.2021.110182.
Tay, Z.Y. (2022a), "Energy generation enhancement of arrays of point absorbers wave energy converters via moonpools' resonance effect", *Renew. Energ.*, https://doi.org/10.1016/j.renene.2022.02.060 (In-Press).
Tay, Z.Y. (2022b), "Power enhancement of wave energy converter array via wave runup in channel", *J. Offshore Mech. Arct. Eng*., **144**(2), 022001, https://doi.org/10.1115/1.4053253.
Tay, Z.Y. and Venugopal, V. (2017a), "Hydrodynamic interactions of oscillating wave surge converters in an array under random sea state", *Ocean Eng.*, **145**, 382-394, https://doi.org/10.1016/j.oceaneng.2017.09.012.
Tay, Z.Y. and Venugopal, V. (2017b), "Optimization of spacing for oscillating wave surge converter arrays using genetic algorithm", *J. Waterw. Port Coast. Ocean Eng.*, **143**(2), 04016019, https://doi.org/10.1061/(ASCE)WW.1943-5460.0000368.
Tay, Z.Y. and Venugopal, V. (2019), "The impact of energy extraction of wave energy converter arrays on wave climate under multi-directional seas", *J. Ocean Eng. Mar. Energ.,* **5**(1), 51-72, https://doi.org/10.1007/s40722-019-00127-w.
Van Rijn, L.C. (2011), 'Coastal erosion and control", *Ocean Coast. Management*, **54**(12), 867-887, https://doi.org/10.1016/j.ocecoaman.2011.05.004.
Venugopal, V., Tay, Z.Y. and Nemalidinne, T.R. (2022), *Numerical Modelling Techniques for Wave Energy Converters in Arrays*, in Ocean Wave Energy Systems, Springer.
Wang, C.M., Yee, A.A., Krock, H. and Tay, Z.Y. (2011), "Research and developments on ocean thermal energy conversion", *The IES J. Part A: Civil & Struct. Eng*., **4**(1), 41-52, https://doi.org/10.1080/19373260.2011.543606.
Wilkinson, L., Whittaker, T.J.T., Thies, P.R., Day, S. and Ingram, D. (2017), "The power-capture of a nearshore, modular, flap-type wave energy converter in regular waves", *Ocean Eng.*, **137**, 394-403, https://doi.org/10.1016/j.oceaneng.2017.04.016.
Williams, A., Geiger, P. and McDougal, W. (1991), "Flexible floating breakwater", *J. Waterw. Port Coast. Ocean Eng.*, **117**(5), 429-450, https://doi.org/10.1061/(ASCE)0733-950X(1991)117:5(429).
Zhao, X., Ning, D., Zou, Q., Qiao, D. and Cai, S. (2019), "Hybrid floating breakwater-WEC system: A review", *Ocean Eng.,* **186**, 106126, https://doi.org/10.1016/j.oceaneng.2019.106126.

ML